

# Dalton Transactions

Accepted Manuscript



This is an *Accepted Manuscript*, which has been through the Royal Society of Chemistry peer review process and has been accepted for publication.

*Accepted Manuscripts* are published online shortly after acceptance, before technical editing, formatting and proof reading. Using this free service, authors can make their results available to the community, in citable form, before we publish the edited article. We will replace this *Accepted Manuscript* with the edited and formatted *Advance Article* as soon as it is available.

You can find more information about *Accepted Manuscripts* in the [Information for Authors](#).

Please note that technical editing may introduce minor changes to the text and/or graphics, which may alter content. The journal's standard [Terms & Conditions](#) and the [Ethical guidelines](#) still apply. In no event shall the Royal Society of Chemistry be held responsible for any errors or omissions in this *Accepted Manuscript* or any consequences arising from the use of any information it contains.



## How a novel tyrosine-heme cross-link fine-tunes the structure and function of heme protein: A direct comparison study in L29H/F43Y myoglobin

Received 00th January 20xx,  
Accepted 00th January 20xx

DOI: 10.1039/x0xx00000x

www.rsc.org/

Dao-Jing Yan,<sup>a,†</sup> Hong Yuan,<sup>b,‡</sup> Wei Li,<sup>b,‡</sup> Yu Xiang,<sup>c</sup> Bo He,<sup>a</sup> Chang-Ming Nie,<sup>a</sup> Ge-Bo Wen,<sup>d</sup> Ying-Wu Lin,<sup>a, d\*</sup> and Xiangshi Tan<sup>b\*</sup>

Heme-protein cross-link is a key post-translational modification (PTM) of heme proteins. Meanwhile, the structural and functional consequences of heme-protein cross-links are not fully understood, due to limited studies on a direct comparison of the same protein with and without the cross-link. Tyr-heme cross-link with a C-O bond is a newly discovered PTM of heme proteins, as spontaneously formed in F43Y myoglobin (Mb) between the Tyr hydroxyl group and heme 4-vinyl group *in vivo*. In this study, we found that with an additional distal His29 introduced in the heme pocket, the double mutant L29H/F43Y Mb can form two distinct forms in different protein purification conditions, with and without the novel Tyr-heme cross-link. By solving the X-ray structure of both forms of L29H/F43Y Mb and spectroscopic studies, we made a direct structural and functional comparison in the same protein scaffold. It revealed that the Tyr-heme cross-link regulates the heme distal hydrogen-bonding network, and fine-tunes not only the spectroscopic and ligand binding properties, but also the protein reactivity. Moreover, the formation of the Tyr-heme cross-link in the double mutant L29H/F43Y Mb was investigated *in vitro*. This study addressed the key issue of how Tyr-heme cross-link fine-tunes the structure and function of heme protein, and provided a plausible mechanism for the formation of the newly discovered Tyr-heme cross-link.

### Introduction

Heme proteins are key metalloproteins in biological systems and perform a large array of functions, including oxygen binding and delivery (e.g. myoglobin, Mb and hemoglobin, Hb), electron transfer (e.g. cytochrome *c*, cyt *c* and cytochrome *b<sub>5</sub>*, cyt *b<sub>5</sub>*), catalysis (e.g. peroxidase and cytochrome P450, CYP450), and signaling (NO sensor soluble guanylate cyclase, sGC, and CO sensor CooA, *etc*).<sup>1-12</sup> Remarkably, heme proteins use the same heme group to confer such diverse functions. This is attributed to various interactions between the heme and the protein matrix, such as the coordination of heme iron by various axial ligands (His, Met, Cys, water, *etc*) and the hydrogen-bonding interactions in the heme distal pocket.<sup>1-12</sup> In addition, post-translational modifications (PTMs) play key roles in tuning the structure and function of heme proteins. Examples include nitration of Tyr/Trp,<sup>13-15</sup> glycosylation of Asn,<sup>16</sup> and formation of cross-links, not only between amino

acids such as Tyr-His in heme-copper oxidase (HCO),<sup>17, 18</sup> but also between the heme and the protein matrix.<sup>19-22</sup>

During the past three decades, a broad diversity of heme-protein cross-links have been discovered, including Cys/SeCys-heme, Met-heme, His-heme, Trp/Tyr-heme, Glu/Asp-heme and Lys-heme cross-links, with bond type ranging from C-S, C-Se, C-N, C-C to C-O.<sup>22</sup> The formation of the diverse heme-protein cross-links has attracted extensive attention. For example, Raven and co-workers showed that introduction of a Cys (S160C mutation) close to the heme 2-vinyl group in recombinant pea cytosolic ascorbate peroxidase (APX) leads to the formation of a thioether bond, during reconstitution of the apo-protein with heme *in vitro* under reducing conditions.<sup>23</sup> When a Met was introduced at the same position, S160M APX was able to form a sulfonium ion bond, with an addition of hydroxyl group at the C<sub>α</sub> of heme vinyl group, by reconstitution of the apo-protein with heme and exposure to H<sub>2</sub>O<sub>2</sub>. Moreover, it was found that this position is suitable for formation of a Tyr-heme cross-link in an autocatalytic reaction of S160Y APX with H<sub>2</sub>O<sub>2</sub>.<sup>24</sup> Meanwhile, there is no X-ray or NMR structural information available for the heme-protein cross-link in S160C, S160M and S160Y APX.

Rational protein design has been proved to be a powerful tool for investigating the structure and function relationship, especially for heme proteins.<sup>1-12</sup> Recently, inspired by the novel His-heme cross-link in truncated Hb family, cyanobacteria *Synechocystis* sp. PCC 6803<sup>25</sup> and *Synechococcus* sp. PCC 7002<sup>26</sup>, Lecomte and co-workers designed a His-heme cross-

<sup>a</sup> School of Chemistry and Chemical Engineering, University of South China, Hengyang 421001, China; E-mail: linlinying@hotmail.com; ywlin@usc.edu.cn

<sup>b</sup> Department of Chemistry/Shanghai Key Lab of Chemical Biology for Protein Research & Institute of Biomedical Science, Fudan University, Shanghai 200433, China; E-mail: xstan@fudan.edu.cn

<sup>c</sup> Department of Chemistry, Tsinghua University, Beijing 100084, China

<sup>d</sup> Laboratory of Protein Structure and Function, University of South China, Hengyang 421001, China.

†Electronic Supplementary Information (ESI) available: Experimental details, MALDI-TOF mass spectra and UV-vis spectra. See DOI: 10.1039/x0xx00000x

\*These authors contributed equally.

link in a eukaryotic globin, *Chlamydomonas eugametos* LI637 (CtrHb).<sup>27</sup> The cross-link can also be introduced in other globins, such as in Mb by introduction of a non-coordinating histidine close to the heme 2-vinyl group (I107H mutation), whereas no structural information of I107H Mb was obtained yet.<sup>28</sup> More recently, we engineered a tyrosine (F43Y mutation) in the heme distal pocket of sperm whale Mb, aiming to tune the binding of exogenous ligands using hydrogen-bonding interaction by the Tyr hydroxyl group. Unexpectedly, the X-ray structure of F43Y Mb revealed that a novel C-O bond was formed between the Tyr hydroxyl group and heme 4-vinyl group,<sup>29</sup> which is different from the Tyr-heme linkage with the C4 atom of porphyrin in heme P460.<sup>30</sup> Moreover, in contrast to the His-heme cross-link in I107H Mb that has almost no influence on protein properties,<sup>28</sup> the presence of Tyr43 in Mb was found to fine-tune both the spectroscopic properties and reactivity as compared to wild-type (WT) Mb. Meanwhile, the impact could be attributed to either the introduction of a distal tyrosine, the formation of the novel Tyr-heme cross-link, or the combination of both.

Despite these advances, the structural and functional consequences of heme-protein cross-links are not fully understood. It is difficult to reveal the impact of a heme-protein cross-link on both structure and function of the same protein with and without a cross-link. This is due to the fact that either the protein was difficult to crystallize with an unsatisfactory yield of heme-protein cross-link,<sup>21, 23, 24, 31-33</sup> or the cross-link was already formed when the protein was produced in cells.<sup>25, 26, 28, 29</sup> Therefore, in order to make a direct comparison of two proteins differed only by a heme-protein cross-link, it is crucial for choosing an ideal protein scaffold that allows regulation of the formation of heme-protein cross-link, as well as easy crystallization of both forms with and without the cross-link.

Mb has been favored as an ideal protein scaffold for heme protein design by modifying the heme active center.<sup>1, 2, 5, 6, 12, 17, 34-39</sup> As shown herein, we found that when an additional distal histidine was introduced in the heme pocket of F43Y Mb by L29H mutation, the double mutant L29H/F43Y Mb can form two distinct forms in different protein purification conditions, with and without the novel Tyr-heme cross-link between Tyr43 and heme 4-vinyl group. Moreover, we successfully crystallized both forms of L29H/F43Y Mb, which allowed us to make direct structural and functional comparisons of these two forms that were differed only by a Tyr-heme cross-link. This study addressed the key issue of how Tyr-heme cross-link fine-tunes the structure and function of heme protein, and provided valuable insights into the formation of the newly discovered PTM of heme proteins.

## Results and discussion

### Structural comparisons

Based on the protein scaffold of F43Y Mb, we introduced an additional distal histidine by L29H mutation to modulate the distal hydrogen-bonding network. The double L29H/F43Y Mb mutant was purified using oxidative and reductive conditions by addition of 1 mM potassium ferricyanide ( $K_3[Fe(CN)_6]$ ) and

dithiothreitol (DTT), respectively (see SI for details). Interestingly, we obtained two different forms of the double mutant, as confirmed by MALDI-TOF mass spectrometry (Fig. S1†). It showed that when L29H/F43Y Mb was purified in oxidative conditions, the observed mass ( $17371.5 \pm 0.5$  Da, Fig. S1A†) was identical to that of the calculated apo-protein (17371 Da). Meanwhile, when the protein was purified in reductive conditions, the observed mass ( $17987.4 \pm 0.5$  Da, Fig. S1B†) was increased by  $\sim 616$  Da, indicating that the heme group (616.5 Da) was covalently linked to the protein matrix. For clarification, this protein form was termed L29H/F43Y Mb-X.

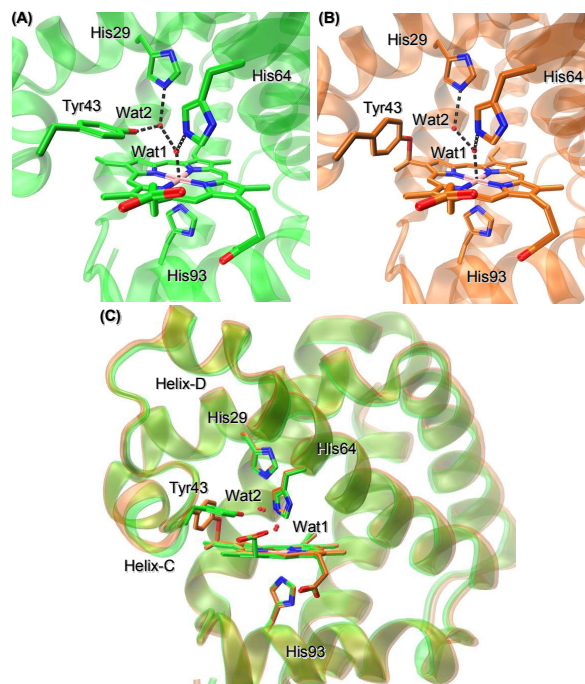


**Fig. 1** Crystal structure of (A) L29H/F43Y Mb showing the heme distal hydrogen-bonding network (dotted lines) (PDB code 4LPI), (B) L29H/F43Y Mb-X showing the Tyr-heme cross-link and altered distal hydrogen-bonding network (PDB code 5C6Y), and (C) overlay of the heme active site of L29H/F43Y Mb (green) with that of L29H/F43Y Mb-X (orange). Helix-C and helix D were labeled for clarification.

We successfully crystallized both L29H/F43Y Mb and L29H/F43Y Mb-X and determined their structures at 1.36 and 1.79 Å resolutions, respectively (Fig. 1, Table S1†). It revealed that there are two distal water molecules (wat1 and wat2, Fig. 1A) in the heme pocket of L29H/F43Y Mb. Wat1 coordinates the heme iron (2.05 Å) and forms two hydrogen bonds with the distal His64 (2.87 Å to the NE2 atom) and wat2 (2.64 Å). Concomitantly, Wat2 forms another two hydrogen bonds with the distal His29 (2.84 Å to the NE2 atom) and Tyr43 (2.20 Å to the hydroxyl oxygen atom). This distal hydrogen-bonding network is similar to that in the X-ray crystal structure of L29H/F43H Mb with three distal histidine residues (PDB code 4FWZ<sup>34</sup>). A hydrogen-bonding network involving a distal Tyr has also been observed in other heme proteins such as in truncated hemoglobin from *Thermobifidafusca*<sup>40</sup> and in the

heme-NO/O<sub>2</sub> binding (H-NOX) domain from *T. tengcongensis*<sup>41</sup>. On the other hand, it revealed that L29H/F43Y Mb-X forms a novel Tyr-heme cross-link between the hydroxyl group of Tyr43 and the heme 4-vinyl group (Fig. 1B). Note that the distance of C-O bond (1.93 Å) is slightly longer than that formed in F43Y Mb (1.58 Å).<sup>29</sup> Consequently, the hydrogen bond between wat2 and Tyr43 was disrupted, and other hydrogen bonds were slightly disturbed, resulting in a distal hydrogen-bonding network similar to that in the single mutant of L29H Mb (PDB code 4IT8<sup>42</sup>).

Moreover, the overall structure of L29H/F43Y Mb was found to overlay well that of L29H/F43Y Mb-X (Fig. 1C). Meanwhile, the conformation of helix C in L29H/F43Y Mb-X was slightly altered, and the side chain of Tyr43 was rotated compared to that in L29H/F43Y Mb. These observations are similar to the overall structure comparison between F43Y Mb and WT Mb.<sup>29</sup> Molecular dynamics simulations revealed that the CD region, where Tyr43 is located, is flexible and controls the dynamics and the ligand binding properties of Mb,<sup>43, 44</sup> which thus allows Tyr43 to link to the heme 4-vinyl group by a conformational change.

### Spectroscopic properties comparisons

With a mere structural difference of Tyr-heme cross-link between L29H/F43Y Mb and L29H/F43Y Mb-X, we made a direct comparison of their spectroscopic properties. It was interesting to find that L29H/F43Y Mb-X exhibited 2-nm blue shifts in the visible spectra in both oxidation states (ferric, met form: 404, 500 and 628 nm; ferrous, deoxy form: 429 and 553 nm) relative to those of L29H/F43Y Mb (ferric, met form: 406, 503 and 630 nm; ferrous, deoxy form: 431 and 555 nm) (Figs. S2A† and S2B†). Therefore, these spectroscopic differences are attributed to the cross-linking between Tyr43 and heme 4-vinyl group. The reduced hemochrome spectrum in pyridine of L29H/F43Y Mb-X showed an  $\alpha$ -band at 553 nm, a 2 nm shift from 555 nm of L29H/F43Y Mb (Fig. S2C†), indicating that one vinyl group of the heme was saturated. In previous studies, similar blue shifts of absorption bands were also reported for the formation of Cys-heme cross-link<sup>45, 46</sup> and His-heme cross-link<sup>27</sup>. These findings thus indicate that the saturation of one vinyl group of the heme results in blue shifts of absorption bands, which is independent of the covalent bond type (C-S, C-N or C-O bond).

When compared to that of WT Mb (409 nm), the Soret band of L29H/F43Y Mb in ferric state (406 nm) shifted 3 nm, which is attributed to the introduction of a distal tyrosine by F43Y mutation, since the single mutant L29H Mb has a Soret band at 409 nm, a same position of WT Mb. The introduction of an electron withdrawing hydroxyl group into heme distal pocket might alter the  $\pi$ - $\pi$  stacking interaction between Phe43 and the heme. Based on these observations, the Soret band difference between F43Y Mb (403 nm) and WT Mb are attributed to both the introduction of a Tyr in the heme distal pocket and the formation of cross-link between Tyr43 and heme 4-vinyl group, with each resulting in a shift of 3 nm.

### Protein stability comparisons

To make a comparison of protein stability as a consequence of Tyr-heme cross-link, we performed Gdn·HCl-induced unfolding studies. It showed that the Soret band of L29H/F43Y Mb decreased with increasing the concentration of Gdn·HCl, and a shoulder peak appeared at  $\sim$ 370 nm of the free heme (Fig. 2A). This observation was similar to that of WT Mb<sup>29</sup> and single mutant L29H Mb (Fig. S3†), suggesting that the heme was released upon unfolding in the absence of a covalent Tyr-heme cross-link. Unfolding study of L29H/F43Y Mb-X showed that the Soret band shifted from 404 to 410 nm in the presence of 5 M Gdn·HCl (Fig. 2B), resulting in a spectrum (410, 534, 564 nm) resembling that of Mb mutants with a bis-His coordination. This observation indicated that the covalent Tyr-heme cross-link in L29H/F43Y Mb-X prevents heme dissociation upon unfolding and leads to a non-native heme state with bis-His coordination.<sup>12, 47</sup> Since this non-native state was also observed for the single mutant F43Y Mb upon unfolding,<sup>29</sup> the distal His64, instead of distal His29, presumably served as one axial ligand of heme in the non-native state, similar to that observed in the X-ray crystal structure of L29E/F43H Mb double mutant.<sup>12</sup>

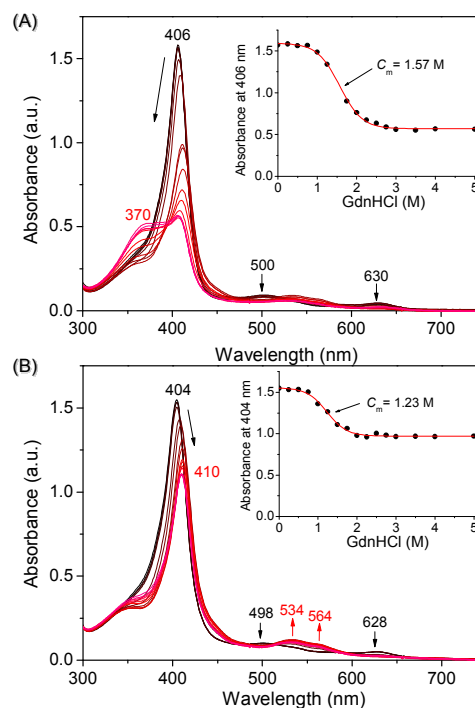


**Fig. 2** UV-visible spectra of Gdn·HCl-induced unfolding of L29H/F43Y Mb (A) and L29H/F43Y Mb-X (B). The changes of Soret band versus Gdn·HCl concentrations were shown as insets.

It should be mentioned that, although the heme group did not dissociate from the protein matrix of L29H/F43Y Mb-X, the heme center was found to be more sensitive to disruptions by Gdn·HCl than that in L29H/F43Y Mb. The half denaturation concentration ( $C_m$ ) for L29H/F43Y Mb-X ( $1.23 \pm 0.03$  M) is 0.24 M lower than that for L29H/F43Y Mb ( $1.57 \pm 0.03$  M) (Table 1). Moreover, a lower  $C_m$  value was observed for F43Y

## ARTICLE

## Dalton Transactions

Mb ( $1.38 \pm 0.04$  M) compared to that for WT Mb ( $1.88 \pm 0.02$  M)<sup>29</sup> and L29H Mb ( $1.84 \pm 0.01$  M) (Fig. S3†, inset). These observations suggest that the hydrogen-bonding interaction by the hydroxyl group of Tyr43 in L29H/F43Y Mb contributes to the heme stability at the initial stage of protein unfolding.

**Table 1.** Comparisons of the half denaturation concentration ( $C_m$ ) of Gdn-HCl, the binding dissociation constant ( $K_D$ ) for imidazole-protein complexes, the rate constant ( $k_1$ ) of compound II formation, and the dissociation rate constant ( $k_{off}$ ) of  $H_2O_2$  for WT Mb and its mutants.

Mbs	$C_m$ (M)	$K_D$ (mM)	$k_1$ ( $mM^{-1}s^{-1}$ )	$k_{off}$ ( $s^{-1}$ )
WT Mb	$1.88 \pm 0.02$	$17.2 \pm 0.6$	$0.57 \pm 0.01$	0
L29H Mb	$1.84 \pm 0.01$	$46.8 \pm 0.9$	$0.44 \pm 0.02$	0
F43Y Mb	$1.38 \pm 0.04$	$2.5 \pm 0.1$	$53.3 \pm 1.1$	0
L29H/F43Y Mb	$1.57 \pm 0.03$	$100.9 \pm 3.6$	$1.15 \pm 0.02$	0.026
L29H/F43Y Mb -X	$1.23 \pm 0.03$	$47.0 \pm 3.6$	$1.06 \pm 0.02$	0.17

### Distal hydrogen-bonding stability comparisons

To further probe the stability difference of distal hydrogen-bonding interactions in L29H/F43Y Mb and L29H/F43Y Mb-X, we used imidazole, instead of fluoride, for competitive ligand binding to the heme iron, since in a recent study we found that fluoride ion could hardly binds to the heme iron in L29H Mb with an additional distal hydrogen-bonding interaction.<sup>48</sup> It showed that upon titration of imidazole at pH 7.0, the Soret band of L29H/F43Y Mb decreased in intensity and shifted from 406 to 409 nm, with a decrease of both 500 and 630 nm absorptions and a concomitant increase of visible band around 532 nm (Fig. 3A). Similar spectral changes were observed for the titration of L29H/F43Y Mb-X (Fig. 3B), as well as the control experiments for WT Mb (Fig. S4A†), L29H Mb (Fig. S4B†) and F43Y Mb (Fig. S4C†), respectively. In case of WT Mb, the resultant spectrum (413, 535 and 565 nm) is nearly identical to that of bis-His coordinated Mb mutants<sup>12, 47</sup> and other *b*-type heme proteins with bis-His coordination such as cyt *b*<sub>5</sub>.<sup>49</sup> These spectral changes indicate that imidazole binds the heme iron and forms a low-spin, six-coordinate protein complex.

To determine the dissociation constant ( $K_D$ ) of imidazole binding, we referenced to the method of Kosowicz and Boon for determining the  $K_D$  of fluoride ion binding to heme proteins.<sup>50</sup> We monitored the spectral changes at 532 nm due to the formation of imidazole-protein complex, and plotted versus imidazole concentrations. As shown in Figs. 3A and 3B, insets, the  $K_D$  was calculated to be  $100.9 \pm 3.6$  mM and  $47 \pm 3.6$  mM for L29H/F43Y Mb and L29H/F43Y Mb-X, respectively. The comparison indicates that imidazole binds more weakly to the heme iron in L29H/F43Y Mb than that in L29H/F43Y Mb-X, which in turn suggests that the distal hydrogen-bonding interaction in L29H/F43Y Mb, with a contribution from Tyr43, is stronger than that in L29H/F43Y Mb-X.

Additional information was obtained from control titration experiments for WT Mb, L29H Mb and F43Y Mb. It was interesting to find that L29H Mb has a  $K_D$  value of  $46.8 \pm 0.9$  mM, which is almost identical to that of L29H/F43Y Mb-X and is  $\sim 2.7$ -fold higher than that of WT Mb ( $17 \pm 0.6$  mM, Table 1).

This observation suggests that the hydrogen-bonding interaction between distal His29 and water2 stabilizes the axial water molecule, whereas distal Tyr43, after forms a cross-link with heme 4-vinyl group, makes no contribution to the stability of distal hydrogen-bonding network. Moreover, F43Y Mb single mutant was found to have a considerable low  $K_D$  value of  $2.5 \pm 0.1$  mM. It suggests that in the absence of distal His29, the Tyr-heme cross-link in F43Y Mb destabilizes the distal hydrogen-bonding network, although with two distal water molecules in the heme pocket of F43Y Mb.<sup>29</sup> This is likely due to the fact that the heme group shifted slightly into the heme pocket with respect to its position in WT Mb as a consequence of linkage to Tyr43,<sup>29</sup> resulting in a weaker distal hydrogen-bonding network involving His64 and two distal water molecules. Note that in presence of the distal His29, the heme group in L29H/F43Y Mb-X overlaps well with that in L29H/F43Y Mb (Fig. 1C).

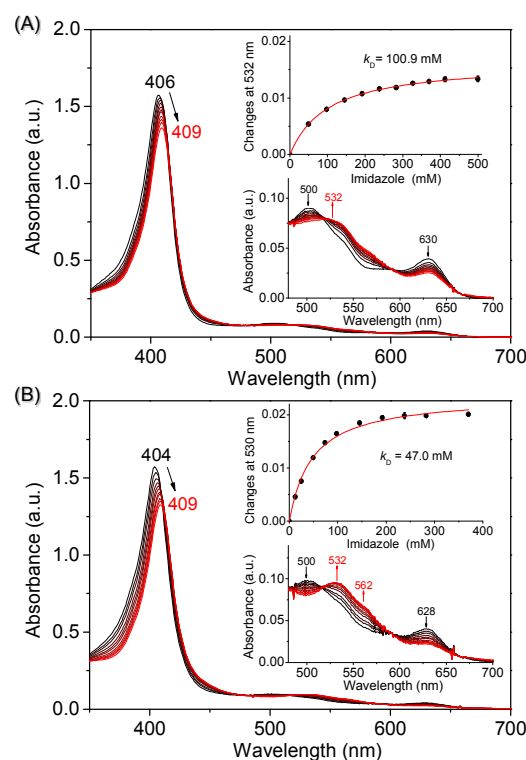


**Fig. 3** UV-vis spectra of L29H/F43Y Mb (A) and L29H/F43Y Mb-X (B) upon titration with imidazole. The fitting of the intensity changes of Soret band versus imidazole concentrations is shown as an inset.

### Hydrogen peroxide activation comparisons

In order to examine the protein reactivity as a consequence of Tyr-heme cross-link, we compared the ability of  $H_2O_2$  activation by L29H/F43Y Mb and L29H/F43Y Mb-X, as well as with the single mutants (L29H Mb and F43Y Mb) and WT Mb. Stopped-flow kinetic studies showed that similar to WT Mb reacting with  $H_2O_2$  (Fig. S5A†), both L29H/F43Y Mb (Fig. S5B†) and L29H/F43Y Mb-X (Fig. 4A) yield an oxoferryl heme (Compound II) species upon reaction with  $H_2O_2$ . Meanwhile, it was different from WT Mb that the decay curve

of Soret band for the double mutant was found to be biphasic, with a rapid first phase (formation of Compound II) and a dominating slower second phase. Since only slight decrease in intensity was observed for the Soret band in the second phase, partial heme degradation was presumably occurred in this phase. We thus calculated the observed rate constant ( $k_{\text{obs}}$ ) from the first phase. It showed that L29H/F43Y Mb-X exhibits slightly enhanced ability towards activation of  $\text{H}_2\text{O}_2$  (Fig. 4B), which may be attributed to a higher protein stability with a Tyr-heme cross-link. In a previous study<sup>51</sup>, Lu and co-workers showed that covalent anchoring of artificial cofactor Mn-salen to apo-Mb improves the rate of thioanisole sulfoxidation using  $\text{H}_2\text{O}_2$  as an oxidant.

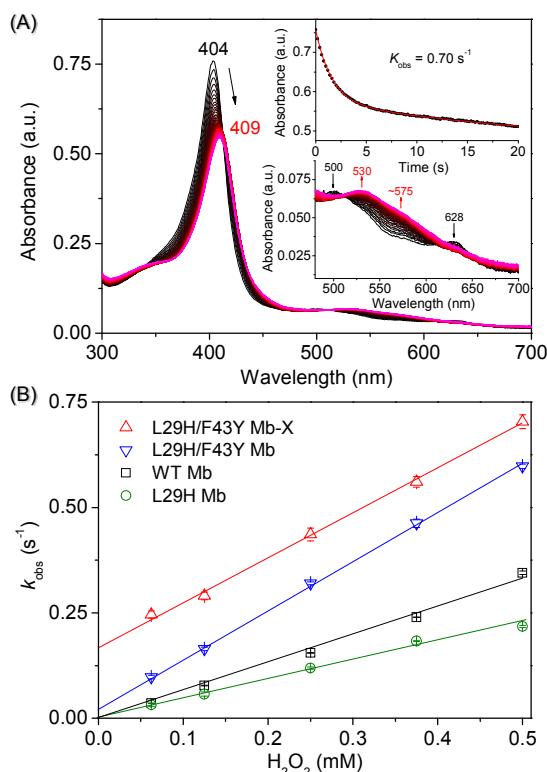


**Fig. 4** Kinetic study of  $\text{H}_2\text{O}_2$  activation. (A) Stopped-flow spectra upon mixing  $10 \mu\text{M}$  L29H/F43Y Mb and  $0.5 \text{ mM}$   $\text{H}_2\text{O}_2$  in  $100 \text{ mM}$   $\text{KH}_2\text{PO}_4$  buffer, pH 7.0,  $25 \text{ }^\circ\text{C}$ , for 1 s. Inset, the single-exponential fit of the decay of Soret band at  $406 \text{ nm}$ ; (B) Plots of observed rate constants versus  $\text{H}_2\text{O}_2$  concentrations. The linear fit yields the apparent rate constant  $k_1$  as the slope of the line.

The rate constant ( $k_1$ ) of Compound II formation, as determined by plot of  $k_{\text{obs}}$  versus  $\text{H}_2\text{O}_2$  concentrations, is  $1.15 \pm 0.02$  and  $1.06 \pm 0.02 \text{ mM}^{-1}\text{s}^{-1}$  for L29H/F43Y Mb and L29H/F43Y Mb-X, respectively (Table 1). The linear plot for L29H/F43Y Mb-X has a positive slope with a value of  $0.17 \text{ s}^{-1}$ , which indicates that some  $\text{H}_2\text{O}_2$  molecules may not react to form compound II and dissociate from the heme center of L29H/F43Y Mb-X. Similarly, Obinger and co-workers<sup>33</sup> observed recently that  $\text{H}_2\text{O}_2$  dissociated faster when the heme was covalently linked to the protein scaffold of a bacterial peroxidase. These observations are likely due to the alteration

of the architecture of distal heme cavity by the heme-protein cross-link. Comparison study showed that the  $k_{\text{off}}$  value is  $\sim 6.5$ -fold than that for L29H/F43Y Mb ( $0.026 \text{ s}^{-1}$ , Table 1). Note that a dissociation of  $\text{H}_2\text{O}_2$  was not observed for WT Mb and the single mutants of L29H Mb and F43Y Mb. These observations suggest that Tyr-heme cross-link in the double mutant fine-tunes not only the protein reactivity, but also the ligand binding properties.

Control experiments revealed that the rate constants of compound II formation for L29H/F43Y Mb and L29H/F43Y Mb-X are only  $\sim 2$ -fold than that for the WT Mb under the same condition ( $0.57 \pm 0.01 \text{ mM}^{-1}\text{s}^{-1}$ ). Note that a similar value ( $0.51 \text{ mM}^{-1}\text{s}^{-1}$  at  $20 \text{ }^\circ\text{C}$ ) was reported for WT Mb by Watanabe and co-workers in previous study.<sup>52</sup> This is distinct from F43Y Mb, as reported previously,<sup>29</sup> exhibiting dramatically enhanced ( $\sim 100$ -fold) ability of  $\text{H}_2\text{O}_2$  activation ( $53.3 \pm 1.1 \text{ mM}^{-1}\text{s}^{-1}$ ). These observations suggest that the rate of compound II formation is mainly regulated by the distal His29 in both L29H/F43Y Mb and L29H/F43Y Mb-X, whereas the Tyr43-heme cross-link has only slight influences. This observation was further supported by the low ability of  $\text{H}_2\text{O}_2$  activation for the single mutant L29H Mb (Fig. S5C†), with a rate constant ( $0.44 \pm 0.02 \text{ mM}^{-1}\text{s}^{-1}$ ) lower than that for WT Mb (Table 1), agreeing with previous observation for L29H/H64L Mb double mutant.<sup>52</sup>

#### Mechanism of Tyr-Heme cross-link

Since L29H/F43Y Mb-X was obtained in purification with air-saturated buffer solution in presence of reductant, DTT ( $1 \text{ mM}$ ), in order to provide information for the mechanism of Tyr-Heme cross-linking, the reaction of L29H/F43Y Mb with DTT was investigated by monitoring the changes in its absorption spectrum in air-saturated solution ( $100 \text{ mM}$   $\text{KH}_2\text{PO}_4$ , pH 7.0). As shown in Fig. 5, after addition of  $1 \text{ mM}$  DTT to L29H/F43Y Mb ( $10 \mu\text{M}$ ) in air, the Soret band of  $406 \text{ nm}$  decreased in intensity, and a shoulder band appeared at  $\sim 430 \text{ nm}$ . The time dependent of these two bands were shown as an inset in Fig. 5 (right top). Concomitantly, the characteristic peaks of met Mb in the visible region ( $502$  and  $630 \text{ nm}$ ) decreased in intensity, and a broad peak at  $\sim 540 \text{ nm}$  appeared, with a shoulder peak at  $\sim 565 \text{ nm}$ . The resultant visible bands resemble that for the oxy-form spectrum of L29H/F43Y Mb ( $540$  and  $\sim 570 \text{ nm}$ , Fig. S6†). These spectral changes indicate that reduction of L29H/F43Y Mb by DTT in presence of  $\text{O}_2$  results in a mixture of deoxy and oxy forms of the protein. It was shown that by addition of a strong oxidant,  $\text{K}_3[\text{Fe}(\text{CN})_6]$ , to the reaction solution, the Soret band of the protein changed to  $404 \text{ nm}$ ,  $2\text{-nm}$  blue-shifted from the original  $406 \text{ nm}$ . Note that the decrease in intensity of the Soret band suggests partial heme degradation in the reaction, similar to that occurs in reaction with  $\text{H}_2\text{O}_2$  (Fig. 4A). Furthermore, the reduced hemochrome spectrum of L29H/F43Y Mb after reaction showed an  $\alpha$  band at  $553 \text{ nm}$  (Fig. S7†), identical to that of L29H/F43Y Mb-X (Fig. 2C). These observations thus indicate that Tyr-heme cross-link was formed by DTT-induced reduction of L29H/F43Y Mb in presence of  $\text{O}_2$ .

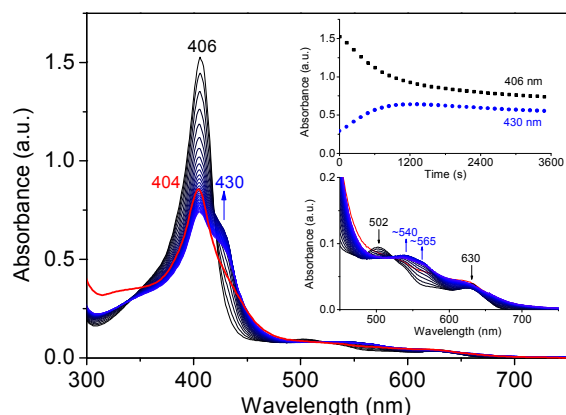


**Fig. 5** Kinetic study of DTT-induced reduction of L29H/F43Y Mb. The top inset shows the changes for the Soret bands (406 and 440 nm for the met and deoxy forms, respectively), and the bottom inset shows the changes for the visible bands. The protein was oxidized back to its ferric state by  $K_3[Fe(CN)_6]$  (red spectrum).

To further provide information for the Tyr-heme cross-link, we performed electron paramagnetic resonance (EPR) studies for DTT-induced reduction of L29H/F43Y Mb in presence of  $O_2$ . As shown in Fig. 6, in the absence of DTT, the met form of L29H/F43Y Mb (0.5 mM) exhibited a high-spin signal at  $g = \sim 5.99$  (line a). Upon reduction by 50 mM DTT for 15 min, the high-spin signal decreased and new EPR signals appeared at  $g = 2.35$ , 2.23 and 1.93 (line b). These large rhombic splitting signals are typical of low-spin ferric heme species,<sup>53</sup> which are similar to those observed for oxidation of bleomycin-Fe(II) complex by  $O_2$ , resulting in low-spin Fe(III) species ( $g = 2.431$ , 2.185 and 1.893).<sup>54</sup> A recent study on reaction of reduced inducible nitric oxide synthase (iNOS) with  $O_2$  also showed dominant low-spin heme signals ( $g = 2.40$  and 2.27), which are attributed to the formation of superoxide and direct coordination to the ferric heme iron.<sup>55</sup> These observations suggest that a superoxide form was presumably formed in reaction of L29H/F43Y Mb with DTT in presence of  $O_2$ . Moreover, the signals of low-spin ferric heme decreased in incubation with DTT for longer times (lines c and d), indicating the conversion of superoxide form to other species that may not be detected by EPR in this reaction. The catalytic cycle of CYP450 shows that a superoxide form is converted to a transient active oxidant, Compound I (an oxoferryl heme  $\pi$ -cation radical).<sup>10</sup> Recently, Hirota and co-workers showed that an oxy complex of cyt *c* may convert to Compound I by receiving an electron from DTT, resulting in oxidation of distal Met80.<sup>56</sup> Therefore, Compound I may also form in the reaction herein and is crucial for Tyr-heme cross-linking.

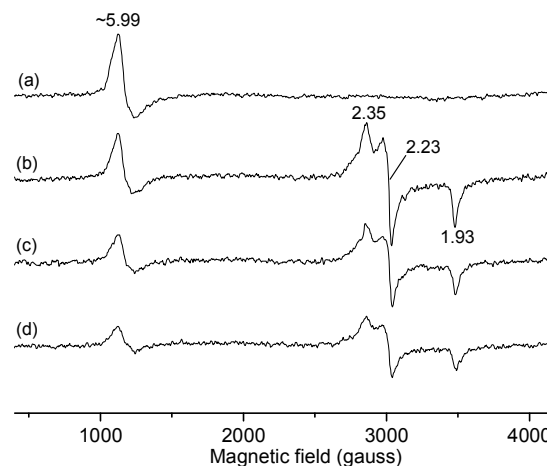
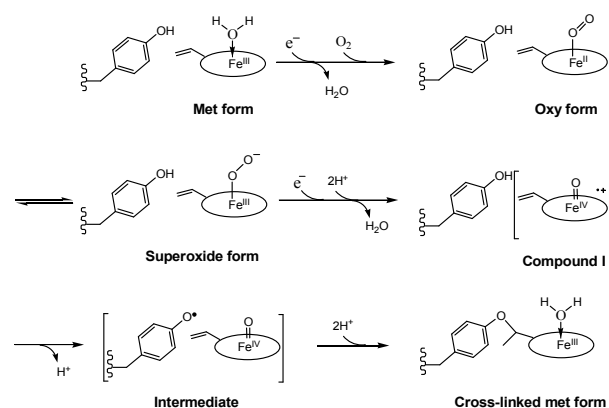


**Fig. 6** EPR spectra of met L29H/F43Y Mb (a), and reduced by DTT in presence of  $O_2$  for 15 min (b), 30 min (c) and 1 hr (d).

Based on above observations, we proposed a mechanism for formation of the Tyr-heme cross-link in L29H/F43Y Mb (Scheme 1). With an electron received from the reductant DTT, the ferric met form of L29H/F43Y Mb is converted to ferrous form, which allows the formation of an oxy-form in air-saturated solution. The oxy complex is equivalent to a low-spin ferric superoxide species, which presumably forms Compound I with an additional electron donated by DTT. Later on, an intermediate of Compound II (oxoferryl heme) with a tyrosyl radical is likely formed through an internal electron transfer from Compound I, as proposed in  $H_2O_2$ -dependent formation of Tyr-heme cross-link with heme porphyrin ring.<sup>24</sup> Finally, a further radical reaction occurs, resulting in formation of a novel Tyr-heme cross-link with the suitably positioned heme 4-vinyl group.

**Scheme 1:** Proposed mechanism for DTT-induced formation of Tyr-heme cross-link in L29H/F43Y Mb.



## Conclusions

In conclusion, we have directly compared the structure and function of two forms of L29H/F43Y Mb that are differed only by a Tyr-heme cross-link via a novel C-O bond. The Tyr-heme cross-link was found to regulate the heme distal hydrogen-bonding network, and fine-tune not only the spectroscopic and ligand binding properties, but also the protein reactivity. DTT-induced reduction of the double mutant in presence of O<sub>2</sub> was shown to result in the formation of Tyr-heme cross-link, which presumably involves the activation of O<sub>2</sub> and formation of catalytic intermediates such as Compounds I and II. In addition to providing new insights into the diverse chemistry of heme PTMs, this study shows that the formation of Tyr-heme cross-link is controllable and can be potentially used to fine-tune both structure and function of heme proteins.

## Acknowledgements

It is a pleasure to acknowledge Prof. S. G. Sligar and Prof. Y. Lu of University of Illinois at Urbana-Champaign, for the kind gift of sperm whale Mb gene. X-ray diffraction data were collected at Shanghai Synchrotron Radiation Facility (SSRF), China. This work was supported by the National Science Foundation of China, NSFC (Nos. 31370812 to Y.-W. Lin, 21472027, 31270869 to X. Tan, and 11275090 to C.-M. Nie), Hunan Provincial Natural Science Foundation for Distinguished Young Scholars (2015JJ1012) and Zhengxiang scholar program of the University of South China to Y.-W. Lin.

## References

1. Y. Lu, N. Yeung, N. Sieracki and N. M. Marshall, *Nature*, 2009, **460**, 855-862.
2. J. Du, M. Sono and J. H. Dawson, *Coord. Chem. Rev.*, 2011, **255**, 700-716.
3. P. S. Coelho, E. M. Brustad, A. Kannan and F. H. Arnold, *Science*, 2013, **339**, 307-310.
4. T. G. Spiro, A. V. Soldatova and G. Balakrishnan, *Coord. Chem. Rev.*, 2013, **257**, 511-527.
5. Y.-W. Lin, E. B. Sawyer and J. Wang, *Chem. Asian. J.*, 2013, **8**, 2534-2544.
6. Y.-W. Lin and J. Wang, *J. Inorg. Biochem.*, 2013, **129**, 162-171.
7. U. Liebl, J.-C. Lambry and M. H. Vos, *Biochim. Biophys. Acta*, 2013, **1834**, 1684-1692.
8. O. Shoji and Y. Watanabe, *J. Biol. Inorg. Chem.*, 2014, **19**, 529-539.
9. K. Oohora and T. Hayashi, *Curr. Opin. Chem. Biol.*, 2014, **19**, 154-161.
10. T. L. Poulos, *Chem. Rev.*, 2014, **114**, 3919-3962.
11. P. A. Sontz, W. J. Song and F. A. Tezcan, *Curr. Opin. Chem. Biol.*, 2014, **19**, 42-49.
12. J.-F. Du, W. Li, L. Li, G.-B. Wen, Y.-W. Lin and X. Tan, *ChemistryOpen*, 2015, **4**, 97-101.
13. F. Yamakura and K. Ikeda, *Nitric Oxide*, 2006, **14**, 152-161.
14. S. Nicolis, A. Pennati, E. Perani, E. Monzani, A. M. Sanangelantoni and L. Casella, *Chem. Eur. J.*, 2006, **12**, 749-757.
15. Y.-W. Lin, X.-G. Shu, K.-J. Du, C.-M. Nie and G.-B. Wen, *Comput. Biol. Chem.*, 2014, **52**, 60-65.
16. G. J. Palm, A. Sharma, M. Kumari, S. Panjekar, D. Albrecht, M. V. Jagannadham and W. Hinrichs, *FEBS J.*, 2014, **281**, 4319-4333.
17. X. Liu, Y. Yu, C. Hu, W. Zhang, Y. Lu and J. Wang, *Angew. Chem. Int. Ed.*, 2012, **124**, 4388-4392.
18. S. Yoshikawa, K. Shinzawa-Itoh, R. Nakashima, R. Yaono, E. Yamashita, N. Inoue, M. Yao, M. J. Fei, C. P. Libeu, T. Mizushima, H. Yamaguchi, T. Tomizaki and T. Tsukihara, *Science*, 1998, **280**, 1723-1729.
19. C. Colas and P. R. Ortiz de Montellano, *Chem. Rev.*, 2003, **103**, 2305-2332.
20. M. Zederbauer, P. G. Furtmuller, S. Brogioni, C. Jakopitsch, G. Smulevich and C. Obinger, *Nat. Prod. Rep.*, 2007, **24**, 571-584.
21. P. R. Ortiz de Montellano, *Drug Metab. Rev.*, 2008, **40**, 405-426.
22. Y.-W. Lin, *Biochim. Biophys. Acta*, 2015, **1854**, 844-859.
23. C. L. Metcalfe, O. Daltrop, S. J. Ferguson and E. L. Raven, *Biochem. J.*, 2007, **408**, 355-361.
24. Z. Pipirou, A. R. Bottrill, D. A. Svistunenko, I. Efimov, J. Basran, S. C. Mistry, C. E. Cooper and E. L. Raven, *Biochemistry*, 2007, **46**, 13269-13278.
25. B. C. Vu, A. D. Jones and J. T. J. Lecomte, *J. Am. Chem. Soc.*, 2002, **124**, 8544-8545.
26. N. L. Scott, C. J. Falzone, D. A. Vuletich, J. Zhao, D. A. Bryant and J. T. J. Lecomte, *Biochemistry*, 2002, **41**, 6902-6910.
27. S. L. Rice, M. R. Preimesberger, E. A. Johnson and J. T. Lecomte, *J. Inorg. Biochem.*, 2014, **141**, 198-207.
28. S. Uppal, S. Salhotra, N. Mukhi, F. K. Zaidi, M. Seal, S. G. Dey, R. Bhat and S. Kundu, *J. Biol. Chem.*, 2015, **290**, 1979-1993.
29. D. J. Yan, W. Li, Y. Xiang, G. B. Wen, Y. W. Lin and X. Tan, *ChemBioChem*, 2015, **16**, 47-50.
30. P. Cedervall, A. B. Hooper and C. M. Wilmot, *Biochemistry*, 2013, **52**, 6211-6218.
31. C. L. Metcalfe, M. Ott, N. Patel, K. Singh, S. C. Mistry, H. M. Goff and E. L. Raven, *J. Am. Chem. Soc.*, 2004, **126**, 16242-16248.
32. G. Battistuzzi, J. Stampfer, M. Bellei, J. Vlasits, M. Soudi, P. G. Furtmuller and C. Obinger, *Biochemistry*, 2011, **50**, 7987-7994.
33. M. Auer, A. Nicolussi, G. Schutz, P. G. Furtmuller and C. Obinger, *J. Biol. Chem.*, 2014, **289**, 31480-31491.
34. K. D. Miner, A. Mukherjee, Y.-G. Gao, E. L. Null, I. D. Petrik, X. Zhao, N. Yeung, H. Robinson and Y. Lu, *Angew. Chem. Int. Ed.*, 2012, **51**, 5589-5592.
35. Y.-W. Lin, J. Wang and Y. Lu, *Sci. China Chem.*, 2014, **57**, 346-355.
36. C. Hu, S. I. Chan, E. B. Sawyer, Y. Yu and J. Wang, *Chem. Soc. Rev.*, 2014, **43**, 6498-6510.
37. Y. Yu, Q. Zhou, L. Wang, X. Liu, W. Zhang, M. Hu, J. Dong, J. Li, X. Lv, H. Ouyang, H. Li, F. Gao, W. Gong, Y. Lu and J. Wang, *Chem. Sci.*, 2015, **6**, 3881-3885.
38. Y.-W. Lin, S. Nagao, M. Zhang, Y. Shomura, Y. Higuchi and S. Hirota, *Angew. Chem. Int. Ed. Engl.*, 2015, **54**, 511-515.
39. M. Bordeaux, V. Tyagi and R. Fasan, *Angew. Chem. Int. Ed.*, 2015, **54**, 1744-1748.
40. A. Bonamore, A. Ilari, L. Giangiacomo, A. Bellelli, V. Morea and A. Boffi, *FEBS J.*, 2005, **272**, 4189-4201.

## ARTICLE

Dalton Transactions

41. P. Pellicena, D. S. Karow, E. M. Boon, M. A. Marletta and J. Kuriyan, *Proc. Natl. Acad. Sci. U. S. A.*, 2004, **101**, 12854-12859.
42. M.-H. Sun, W. Li, J.-H. Liu, G.-B. Wen, X. Tan and Y.-W. Lin, *RSC Advances*, 2013, **3**, 9337.
43. Y.-W. Lin, *Proteins*, 2011, **79**, 679-684.
44. I. Boron, L. Capece, F. Pennacchietti, D. E. Wetzler, S. Bruno, S. Abbruzzetti, L. Chisari, F. J. Luque, C. Viappiani, M. A. Marti, D. A. Estrin and A. D. Nadra, *Biochim. Biophys. Acta*, 2015, **1850**, 169-177.
45. P. D. Barker, J. C. Ferrer, M. Mylrajan, T. M. Loehr, R. Feng, Y. Konishi, W. D. Funk, R. T. MacGillivray and A. G. Mauk, *Proc. Natl. Acad. Sci. U. S. A.*, 1993, **90**, 6542-6546.
46. Y.-W. Lin, W.-H. Wang, Q. Zhang, H.-J. Lu, P.-Y. Yang, Y. Xie, Z.-X. Huang and H.-M. Wu, *ChemBioChem*, 2005, **6**, 1356-1359.
47. Y. Dou, S. J. Admiraal, M. Ikeda-Saito, S. Krzywda, A. J. Wilkinson, T. Li, J. S. Olson, R. C. Prince, I. J. Pickering and G. N. George, *J. Biol. Chem.*, 1995, **270**, 15993-16001.
48. J. Zeng, Y. Zhao, W. Li, X. Tan, G.-B. Wen and Y.-W. Lin, *J. Mol. Catal. B: Enzym.*, 2015, **111**, 9-15.
49. R. C. Durley and F. S. Mathews, *Acta Crystallogr. D Biol. Crystallogr.*, 1996, **52**, 65-76.
50. J. G. Kosowicz and E. M. Boon, *J. Inorg. Biochem.*, 2013, **126**, 91-95.
51. J. R. Carey, S. K. Ma, T. D. Pfister, D. K. Garner, H. K. Kim, J. A. Abramite, Z. Wang, Z. Guo and Y. Lu, *J. Am. Chem. Soc.*, 2004, **126**, 10812-10813.
52. T. Matsui, S. Ozaki, E. Liong, G. N. Phillips, Jr. and Y. Watanabe, *J. Biol. Chem.*, 1999, **274**, 2838-2844.
53. D. A. Svistunenko, B. J. Reeder, M. M. Wankasi, R. L. Silaghi-Dumitrescu, C. E. Cooper, S. Rinaldo, F. Cutruzzola and M. T. Wilson, *Dalton transactions*, 2007, 840-850.
54. Y. Sugiura, *J. Am. Chem. Soc.*, 1980, **102**, 5208-5215.
55. V. Berka, W. Liu, G. Wu and A. L. Tsai, *J. Inorg. Biochem.*, 2014, **139**, 93-105.
56. Z. Wang, Y. Ando, A. D. Nugraheni, C. Ren, S. Nagao and S. Hirota, *Molecular bioSystems*, 2014, **10**, 3130-3137.



# How a novel tyrosine-heme cross-link fine-tunes the structure and function of heme protein: A direct comparison study in myoglobin

Dao-Jing Yan<sup>a†</sup>, Hong Yuan<sup>b†</sup>, Wei Li<sup>b†</sup>, Yu Xiang<sup>c</sup>, Bo He,<sup>a</sup> Chang-Ming Nie,<sup>a</sup>

Ge-Bo Wen<sup>d</sup>, Ying-Wu Lin<sup>a, d\*</sup>, and Xiangshi Tan<sup>b\*</sup>

## Contents

### 1. Experimental sections

1.1 Protein preparation	p. S3
1.2 MALDI-TOF mass spectrometry	p. S3
1.3 X-ray crystallography	p. S4
1.4 UV-vis spectroscopy	p. S5
1.5 Gdn·HCl-induced unfolding study	p. S5
1.6 Imidazole binding study	p. S6
1.7 Peroxidase reaction kinetics	p. S6
1.8 EPR spectroscopy	p. S7

2. **Figure S1.** MALDI-TOF mass spectra of L29H/F43Y Mb and L29H/F43Y Mb-X.  
p. S9

3. **Figure S2.** UV-vis spectra comparison of L29H/F43Y Mb and L29H/F43Y Mb-X.  
p. S10

4. **Figure S3.** UV-visible spectra of Gdn·HCl-induced unfolding of L29H Mb.  
p. S11

- 5. Figure S4.** UV-vis spectra of WT Mb, L29H Mb and F43Y Mb upon titration with imidazole. p. S12-13
- 6. Figure S5.** Stopped-flow spectra of WT Mb, L29H/F43Y Mb-X and L29H Mb mixed with H<sub>2</sub>O<sub>2</sub>. p. S14-15
- 7. Figure S6.** UV-vis spectrum of the visible bands for L29H/F43Y Mb in oxy form. p. S16
- 8. Figure S7.** UV-vis spectra of the reduced pyridine hemochromagen complex of L29H/F43Y Mb after reaction. p. S16
- 9. Table S1.** X-ray crystallography data collection and refinement statistics. p. S17

## 1. Experimental section

### 1.1 Protein preparation

WT sperm whale Mb was expressed in BL21(DE3) cells using the Mb gene of pMbt7-7 and purified using the procedure described previously [1]. L29H Mb and F43Y Mb single mutants were expressed and purified as described in previous studies [2, 3]. L29H/F43Y Mb gene was constructed by using the QuickChange Site Directed Mutagenesis Kit (Stratagene), and the double mutations were confirmed by DNA sequencing assay. L29H/F43Y Mb was expressed using a similar procedure as that for WT Mb, L29H Mb and F43Y Mb. Two different forms of L29H/F43Y Mb were obtained in protein purification when the condition was kept in oxidative or reductive state by adding 1 mM potassium ferricyanide ( $K_3[Fe(CN)_6]$ ) or dithiothreitol (DTT), respectively. The form purified in oxidative condition was found to have no Tyr-heme cross-link, termed L29H/F43Y Mb, whereas the other form purified in reductive condition was found to have a novel Tyr-heme cross-link similar to that in F43Y Mb, termed L29H/F43Y Mb-X for clarification. Protein concentration was determined with an extinction coefficient of  $\epsilon_{404} = 157 \pm 3 \text{ mM}^{-1} \cdot \text{cm}^{-1}$  for L29H/F43Y Mb and  $\epsilon_{406} = 155 \pm 3 \text{ mM}^{-1} \cdot \text{cm}^{-1}$  for L29H/F43Y Mb-X, respectively, as calculated using the standard hemochromagen method [4].

### 1.2 MALDI-TOF mass spectrometry

Protein mass spectrum measurement was carried out on an AXIMA Performance MALDI-TOF/TOF mass spectrometer (Shimadzu Corp., Kyoto, Japan).

The matrix used for sample treatment in the MALDI-TOF MS measurement was 10 mg/mL sinapinic acid in 50:50 water/acetonitrile with 0.1% TFA. A mixture of 0.5  $\mu$ L L29H/F43Y Mb and L29H/F43Y Mb-X solution (0.1 mM) and 2  $\mu$ L matrix solution was dropped on a standard sample plate. After dried under ambient condition, the plate was transferred into the mass spectrometer chamber for measurement under positive mode.

### 1.3 X-ray crystallography

L29H/F43Y Mb and L29H/F43Y Mb-X, both with a high purity ( $A_{\text{soret}}/A_{280\text{nm}} > 4.0$ ), were exchanged into 20 mM  $\text{KH}_2\text{PO}_4$  (pH 7.0) and concentrated to  $\sim 1.5$  mM. The vapor diffusion hanging drop technique was used to crystallize the protein under the similar conditions to that for F43Y Mb in previous study [3]. Diffraction data was collected from a single crystal at Shanghai Synchrotron Radiation Facility (SSRF) BL17U beamline, China, using a MAR mosaic 225 CCD detector with a wavelength of 0.9793  $\text{\AA}$  at 100 K. The diffraction data were processed and scaled with HKL-2000 [5]. The structure was solved by the molecular replacement method and the 1.6  $\text{\AA}$  structure of WT Mb (PDB entry 1JP6 [6]) was used as the starting model. Manual adjustment of the model was carried out using the program COOT [7] and the models were refined by PHENIX [8] and Refmac5 [9]. Stereochemical quality of the structures was checked by using PROCHECK [10]. All of residues locate in the favored and allowed region and none in the disallowed region.

#### ***1.4 UV-vis spectroscopy***

UV-vis spectra of L29H/F43Y Mb and L29H/F43Y Mb-X were recorded in 100 mM  $\text{KH}_2\text{PO}_4$  (pH 7.0) on a Hewlett-Packard 8453 diode array spectrometer. Deoxy proteins were prepared by addition of a small amount of sodium dithionite in anaerobic conditions. The pyridine hemochrome spectrum was obtained by using 10  $\mu\text{M}$  proteins in 19 % (vol/vol) pyridine and 0.15 M NaOH, and the protein was reduced by a small amount of sodium dithionite. The reduction of ferric L29H/F43Y Mb (10  $\mu\text{M}$ ) by 1 mM DTT in air-saturated 100 mM  $\text{KH}_2\text{PO}_4$  (pH 7.0) was performed by monitoring the UV-vis spectra changes for 1 hour, and the protein was oxidized back to its ferric state by addition of a small amount of  $\text{K}_3[\text{Fe}(\text{CN})_6]$ . Deoxy L29H/F43Y Mb was prepared by addition of a small amount of sodium dithionite and eluted from PD-10 column (GE Healthcare). The protein was then diluted into  $\text{O}_2$ -saturated 100 mM  $\text{KH}_2\text{PO}_4$  (pH 7.0).

#### ***1.5 Gdn-HCl-induced unfolding study***

Guanidine hydrochloride (Gdn-HCl)-induced unfolding of L29H/F43Y Mb and L29H/F43Y Mb-X were performed by addition of 10  $\mu\text{L}$  protein solution to 2 mL Gdn-HCl stock solutions (0-5.0 M, pH 7.0) to a final concentration of 10  $\mu\text{M}$ . The samples were incubated 25 °C for 30 min before collecting the UV-vis spectra. Control experiment was also performed for single mutant L29H Mb. Gdn-HCl-induced unfolding studies of single mutant F43Y Mb and WT Mb were reported in previous study [3]. The denaturation midpoints ( $C_m$  values) were

calculated by fitting the absorbance of Soret band versus the concentrations of Gdn·HCl to the two-state Boltzmann function (eq. 1).

$$A = A_2 + (A_1 - A_2)/(1 + e^{(C - C_m)/dC}) \quad (1)$$

Here,  $A$  is the absorbance of Soret band;  $A_1$  and  $A_2$  are the initial and final absorbance of Soret band, respectively;  $C$  is the concentration of Gdn·HCl.

### 1.6 Imidazole binding study

L29H/F43Y Mb and L29H/F43Y Mb-X (10  $\mu$ M) were dissolved in 20 mM  $\text{KH}_2\text{PO}_4$  (pH 7.0) and titrated with imidazole at 25  $^\circ\text{C}$ . The UV-Vis spectra were recorded in a range of 300-700 nm with dropwise addition of imidazole. Control experiments were performed for single mutants F43Y Mb and L29H Mb, as well as WT Mb under the same conditions. The dependency of the visible band change ( $\Delta A$ ) due to the formation of His/Imidazole coordination on concentrations of imidazole was analyzed by the following equation (eq. 2):

$$\Delta A = \Delta A_{\max} [(C_P + C_L + K_D - [(C_P + C_L + K_D)^2 - 4C_P C_L]^{1/2})] / 2C_P \quad (2)$$

Here,  $\Delta A$  is the absorbance difference for the visible band;  $\Delta A_{\max}$  is the maximum absorbance difference with ferric heme fully occupied by imidazole;  $C_P$  and  $C_L$  are the total protein and total imidazole concentration, respectively; and  $K_D$  is the equilibrium dissociation constant.

### 1.7 Peroxidase reaction kinetics

The reactions of L29H/F43Y Mb and L29H/F43Y Mb-X with hydrogen

peroxide ( $\text{H}_2\text{O}_2$ ) were determined using a dual mixing stopped-flow spectrophotometer (SF-61DX2 Hi-Tech KinetAsyst™). Typically, one syringe contains 10  $\mu\text{M}$  of protein (in 100 mM  $\text{KH}_2\text{PO}_4$  buffer, pH 7.0), and the second syringe contains  $\text{H}_2\text{O}_2$  with concentration ranging from 0.125 to 1 mM. The reaction was started with mixing of equal volume of solutions from the both syringes. 100 time-dependent spectra were collected over 20-50 sec from 350 to 700 nm at 25 °C. The time traces of Soret band absorbance were biphasic for the double and single mutants. The corresponding pseudo-first-order rate constants,  $k_{\text{obs1}}$  and  $k_{\text{obs2}}$ , were calculated by fitting to double-exponential decay function (eq. 3), and  $k_{\text{obs1}}$  was used for comparison. For WT Mb, the observed rate constants ( $k_{\text{obs}}$ ,  $\text{s}^{-1}$ ) were calculated from single-exponential fits.

$$y = y_0 + ae^{-k_1t} + ae^{-k_2t} \quad (3)$$

The apparent rate constant,  $k_1$  ( $\text{mM}^{-1}\text{s}^{-1}$ ), was obtained by linear regression fitting the plot of the observed rate constants,  $k_{\text{obs}}$ , versus the concentrations of  $\text{H}_2\text{O}_2$  (eq. 4).

$$k_{\text{obs}} = k_{\text{off}} + k_1[\text{H}_2\text{O}_2] \quad (4)$$

where  $k_{\text{off}}$  represents the dissociation rate constant of the Mb- $\text{H}_2\text{O}_2$  complex.

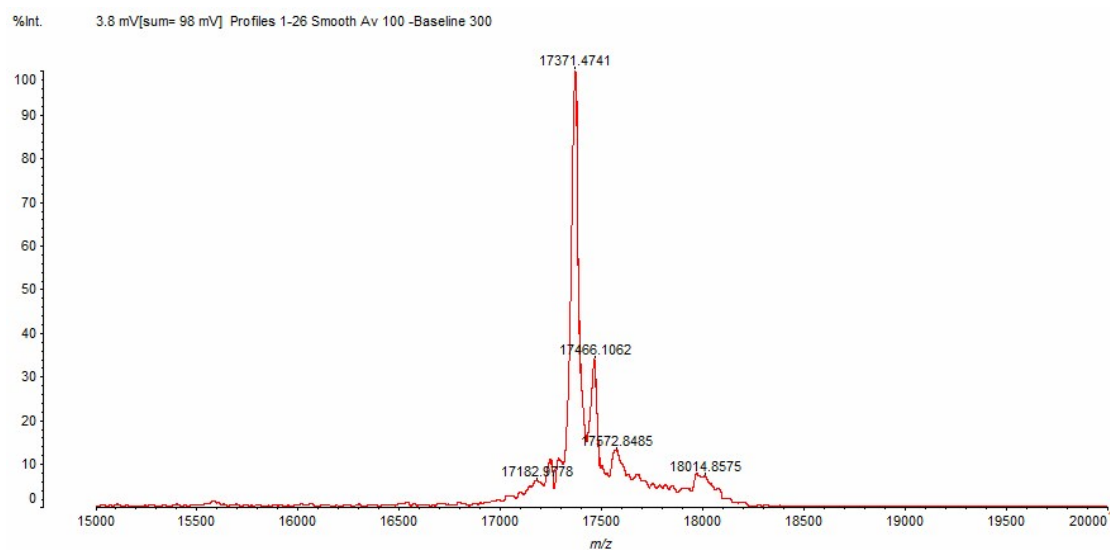
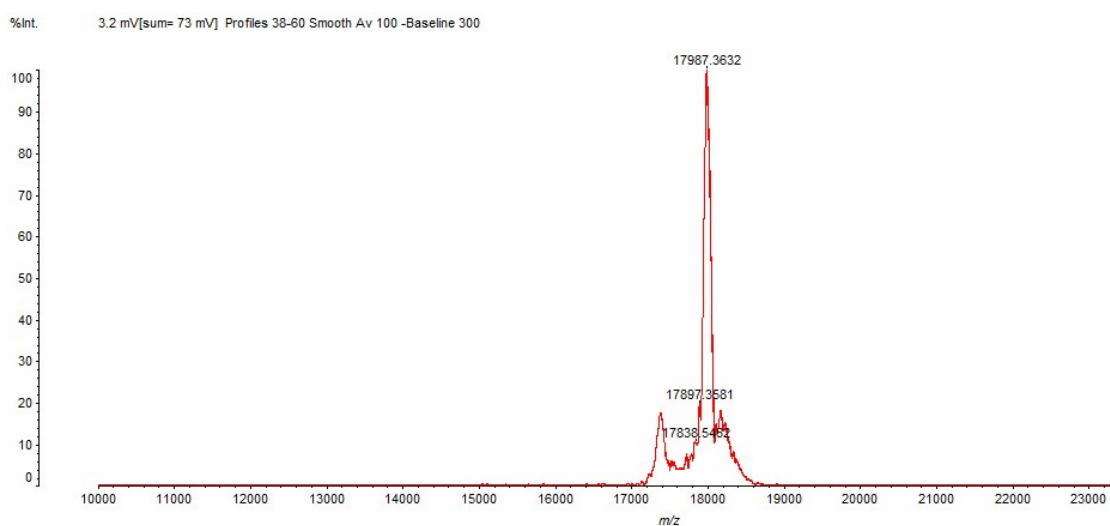
### 1.8 EPR spectroscopy

Electron Paramagnetic Resonance (EPR) spectra of L29H/F43Y Mb was recorded on a Bruker A300 spectrometer (X-band) equipped with Bruker ER4141VTM liquid nitrogen system. The protein sample (0.5 mM in 100 mM

KH<sub>2</sub>PO<sub>4</sub>, pH 7.0) was transferred into an EPR tube with a volume of 300 μL. The spectra were measured at 90 K, with frequency of 9.43 GHz, center field 2200 G and sweep width 3600 G, microwave power 0.595 mW and modulation amplitude 3.0 G. EPR spectra of L29H/F43Y Mb (0.5 mM) after addition of DTT (50 mM) were recorded under the similar condition for 15, 30 and 60 min, respectively.

### References:

- [1] A. Springer, S. G. Sligar. *Proc. Natl. Acad. Sci. USA*, **1987**, 84: 8961-8965.
- [2] M.-H. Sun, W. Li, J.-H. Liu, G.-B. Wen, X. Tan, Y.-W. Lin, *RSC Adv.* **2013**, 3: 9337-9343.
- [3] D.-J. Yan, W. Li, Y. Xiang, G.-B. Wen, Y.-W. Lin, X. Tan. *ChemBioChem*, **2015**, 16:47-50.
- [4] M. Morrison, S. Horie. *Anal. Biochem.* **1965**, 12: 77-82.
- [5] Z. Otwinowski and W. Minor, *Methods Enzymol.* **1997**, 276: 307-326.
- [6] P. Urayama, G. N. Jr Phillips and S. M. Gruner, *Structure*, **2002**, 10: 51–60.
- [7] P. Emsley and K. Cowtan, *Acta Crystallogr. Sect D*, **2004**, 60: 2126-2132.
- [8] P. D. Adams, R. W. Grosse-Kunstleve, L. W. Hung, T. R. Ioerger, A. J. McCoy, N. W. Moriarty, R. J. Read, J. C. Sacchettini, N. K. Sauter and T. C. Terwilliger, *Acta Crystallogr. Sect D*, **2002**, 58: 1948-1954.
- [9] G. N. Murshudov, A. A. Vagin and E. J. Dodson, *Acta Crystallogr. Sect D*, **1997**, 53: 240-255.
- [10] R. A. Laskowski, M. W. MacArthur, D. S. Moss and J. M. Thornton, *J. Appl. Cryst.* **1993**, 26: 283-291.

**(A)****(B)**

**Figure S1.** MALDI-TOF mass spectra of L29H/F43Y Mb (A, Calculated apo-protein, 17371 Da; Observed: 17371.5 Da), and L29H/F43Y Mb-X (B, Calculated holo-protein: 17987 Da; Observed: 17987.4 Da).

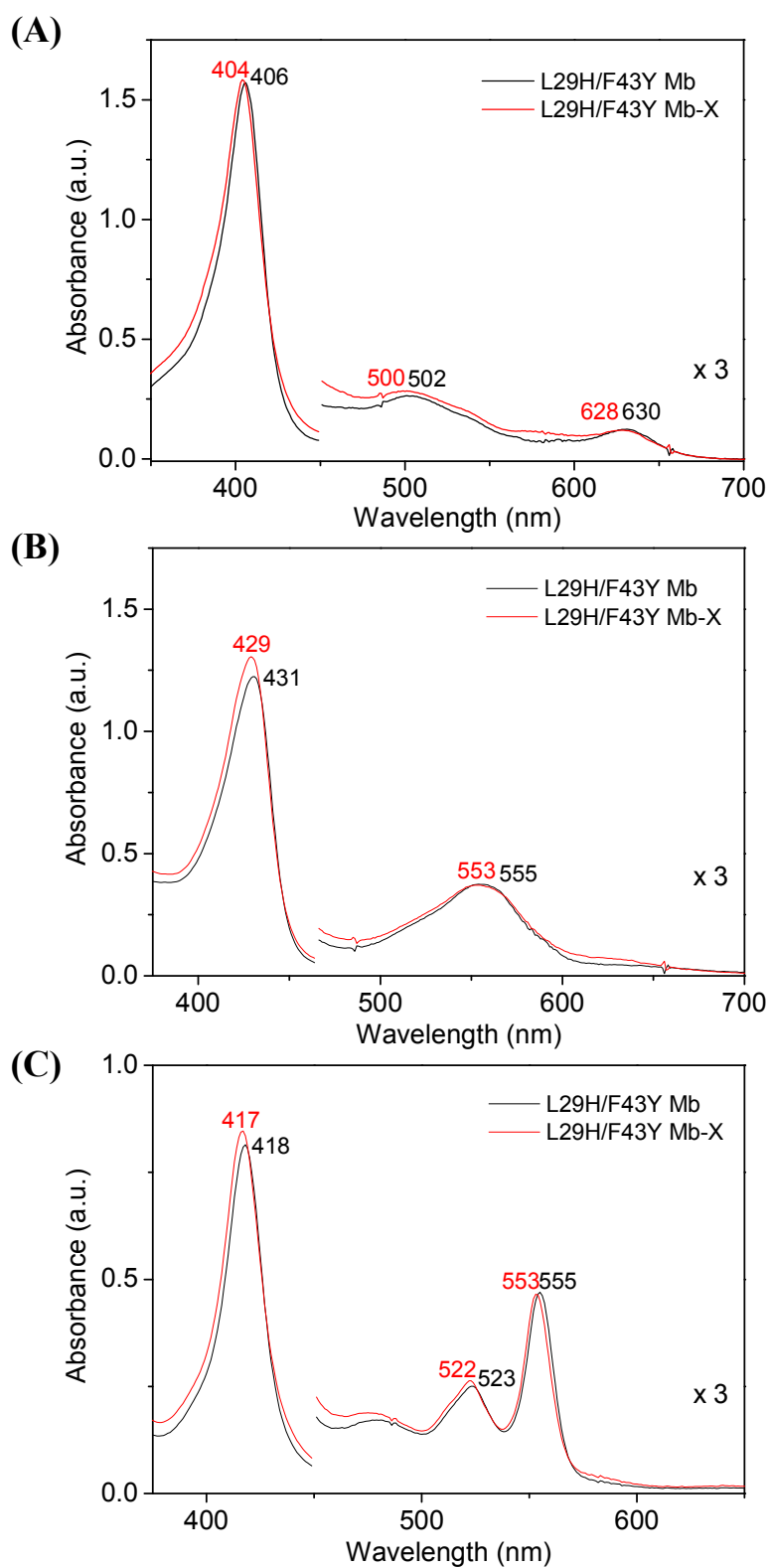


**Figure S2.** UV-vis spectra comparison of L29H/F43Y Mb (black) and L29H/F43Y Mb-X (red) in met form (A), deoxy form (B), and in the reduced pyridine hemochromagen complexes (C).

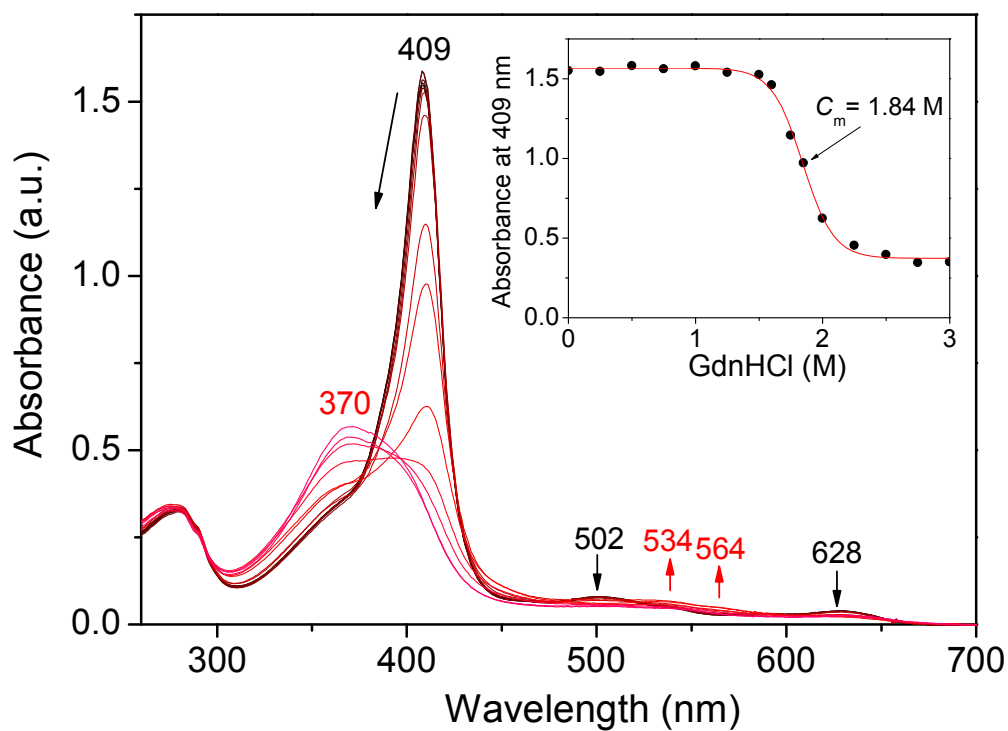
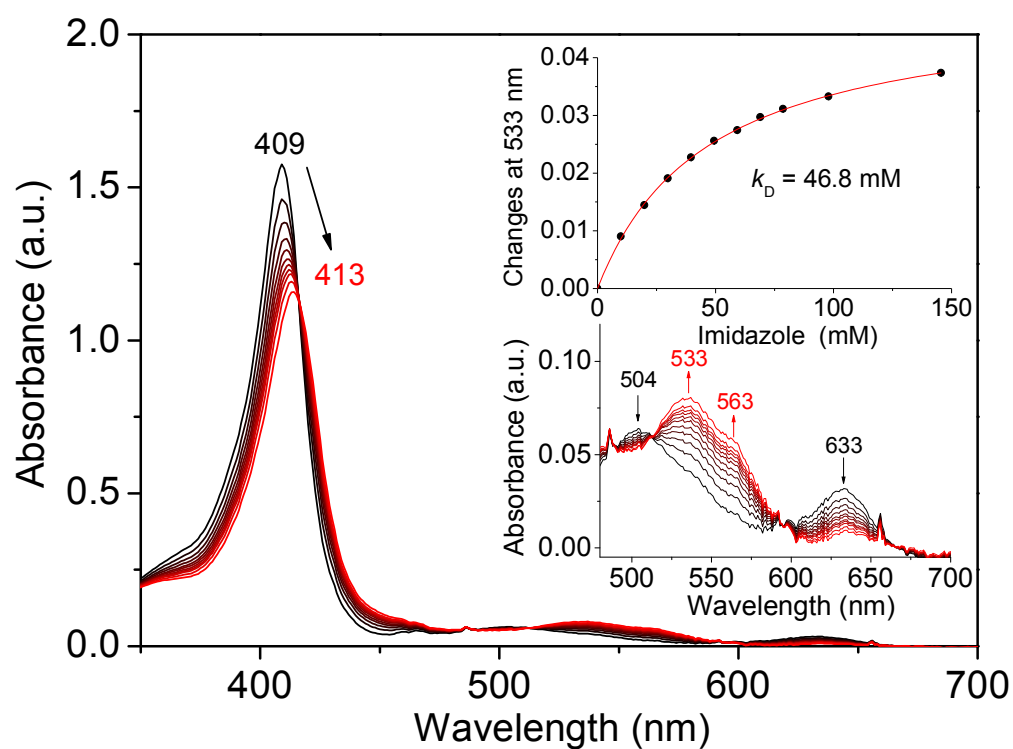
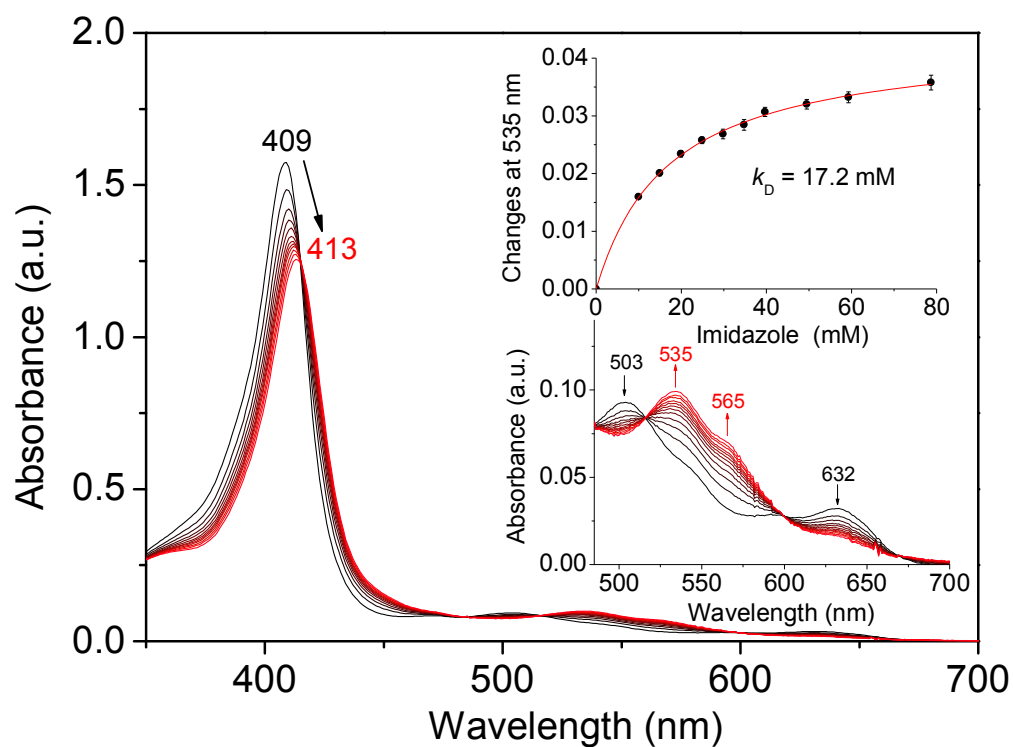


**Figure S3.** UV-visible spectra of Gdn-HCl-induced unfolding of L29H Mb. The changes of Soret band versus Gdn-HCl concentrations were shown as insets.

(A)



(C)

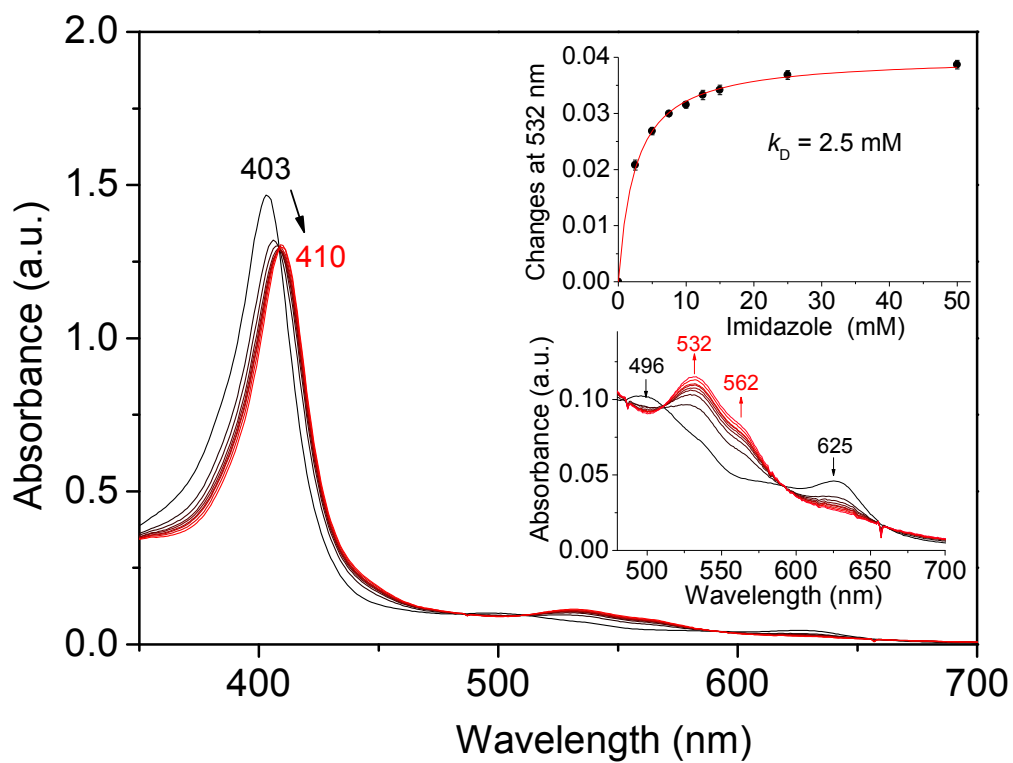
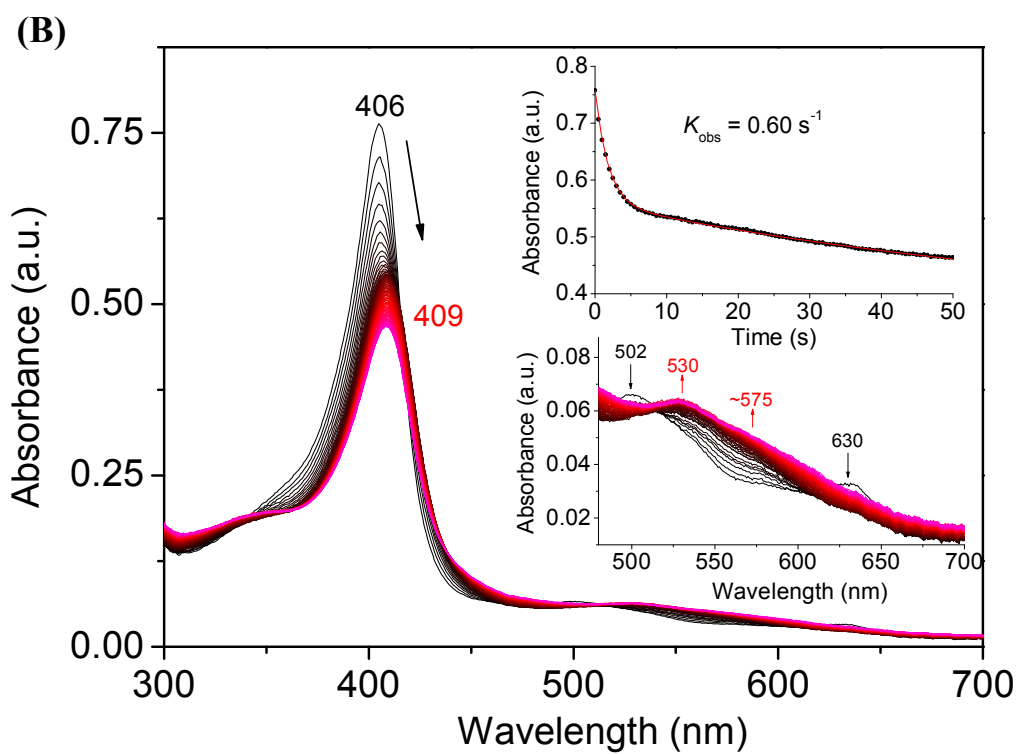
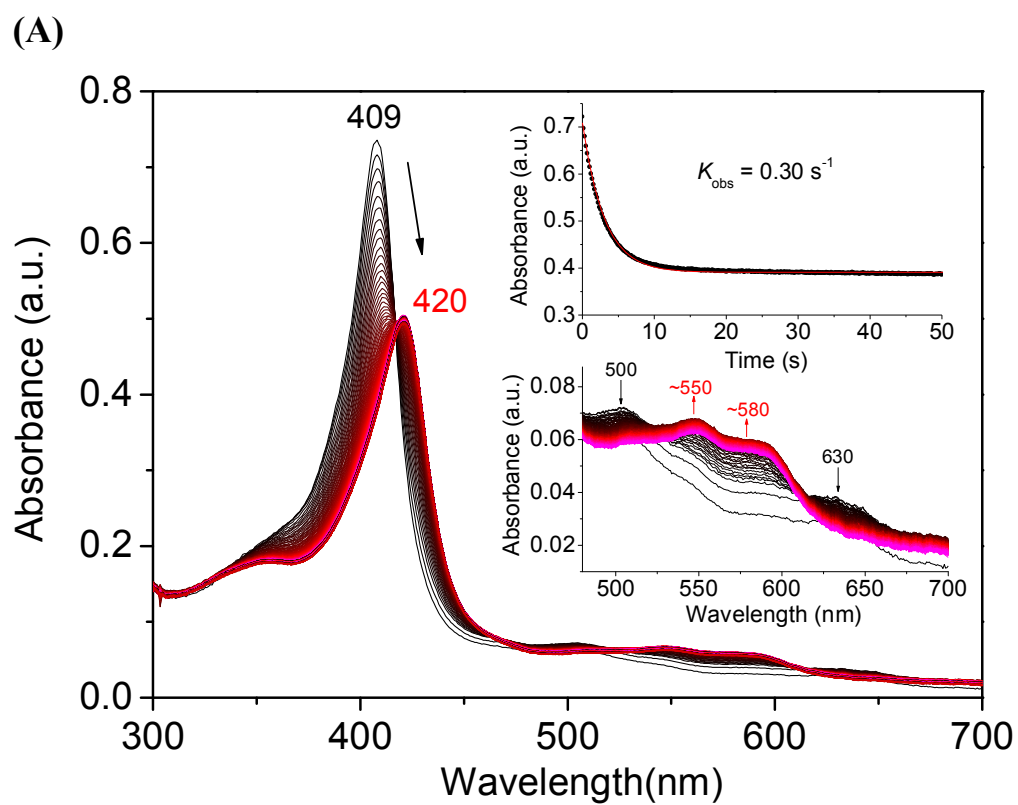


**Figure S4.** UV-vis spectra of WT Mb (A), L29H Mb (B), and F43Y Mb (C) upon titration with imidazole. The fitting of the intensity changes of Soret band versus imidazole concentrations is shown as an inset.



(C)

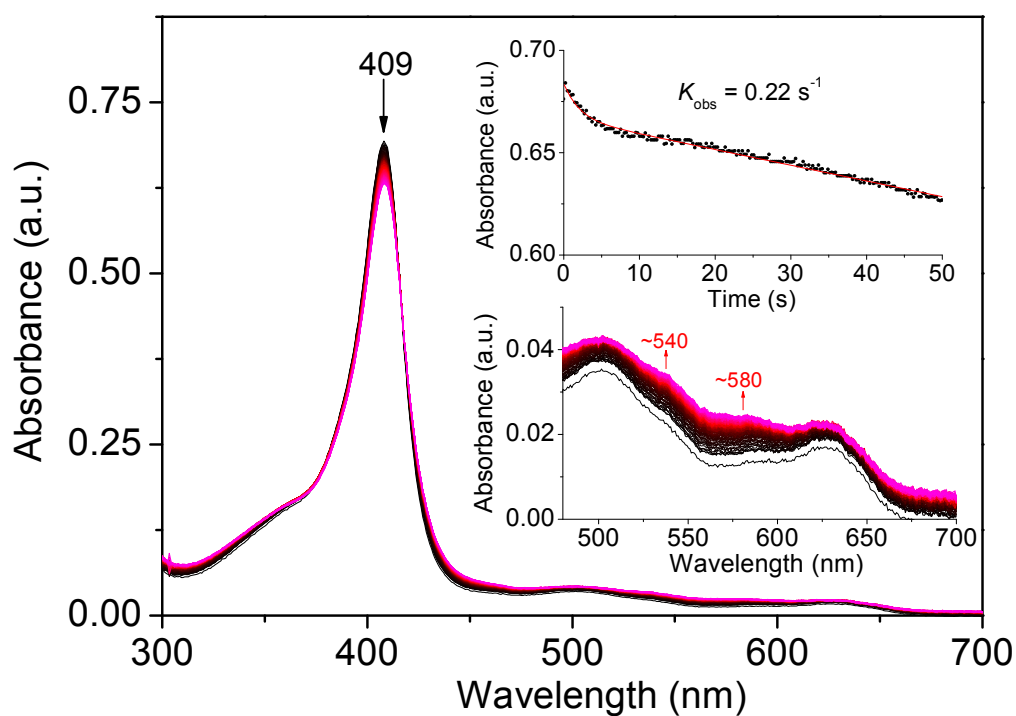


**Figure S5.** Stopped-flow spectra upon mixing 10  $\mu\text{M}$  WT Mb (A), L29H/F43Y Mb-X (B) and L29H Mb (C) and 0.5 mM  $\text{H}_2\text{O}_2$  in 100 mM  $\text{KH}_2\text{PO}_4$  buffer, pH 7.0, 25  $^\circ\text{C}$ , for 20 sec. Insets, the single-exponential fits (A) and double-exponential fit (B and C) of the decay of Soret band.

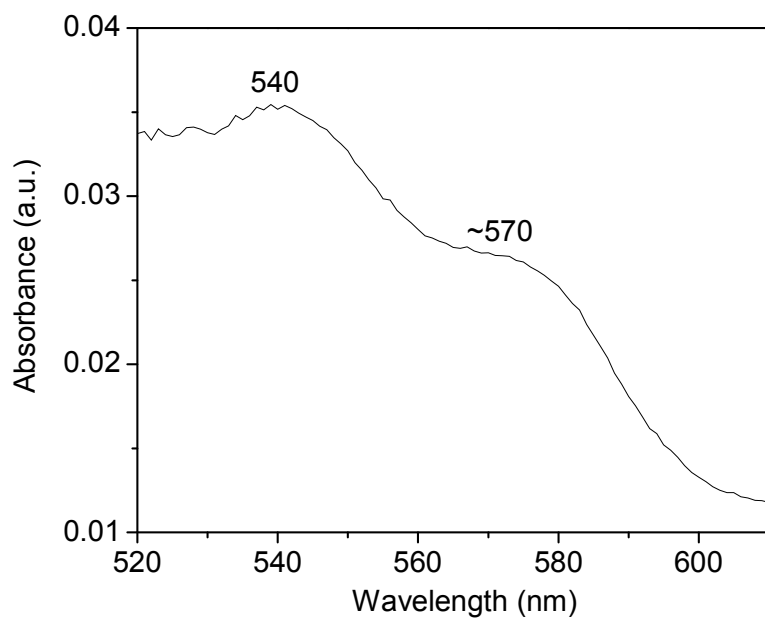


**Figure S6.** UV-vis spectrum of the visible bands for L29H/F43Y Mb in oxy form.

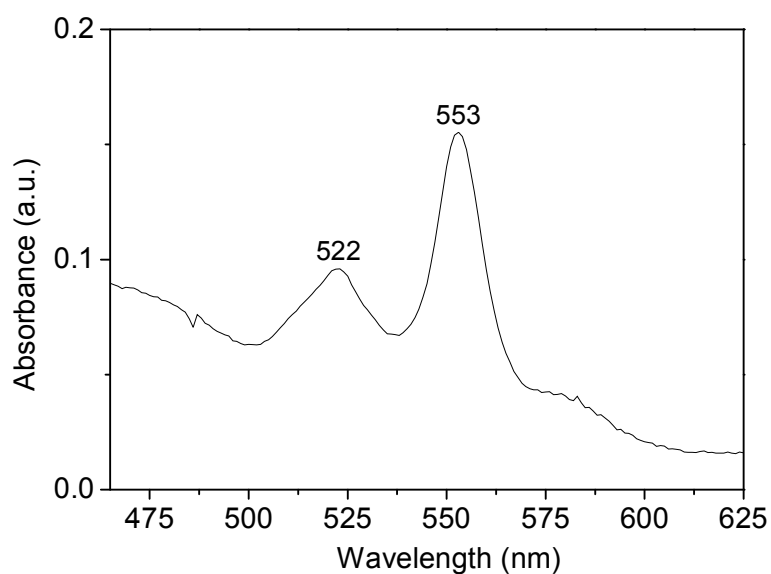


**Figure S7.** UV-vis spectra of the reduced pyridine hemochromagen complex of L29H/F43Y Mb after reaction. The protein was obtained by reaction with DTT in presence of  $O_2$  and re-oxidized by  $K_3[Fe(CN)_6]$ .

**Table S1.** X-ray crystallography data collection and refinement statistics.

	<b>L29H/F43Y Mb</b>	<b>L29H/F43Y Mb-X</b>
Wavelength	0.9792	0.9792
Space group	$P2_12_12_1$	$P2_12_12_1$
Unit-cell dimensions (Å, °)	$a = 39.871, b = 48.400,$ $c = 78.787;$ $\alpha = \beta = \gamma = 90$	$a = 40.062, b =$ $48.348,$ $c = 79.141;$ $\alpha = \beta = \gamma = 90$
Resolution (Å)	1.36	1.79
No. of observations	427643	541169
No. of unique reflections <sup>[a]</sup>	33291 (1638)	14678 (738)
Completeness (%)	99.9 (100.0)	99.7 (100.0)
$\langle I \rangle / (I)$	16.1 (2.0)	19.8 (10.1)
Redundancy	12.8 (12.8)	13.0 (12.9)
$R_{\text{sym}}$ <sup>[b]</sup>	0.068 (0.466)	0.163 (0.524)
$R_{\text{cryst}}$ <sup>[c]</sup> (%) / $R_{\text{free}}$ <sup>[d]</sup> (%)	0.1801 / 0.1991	0.1568 / 0.1808
RMSD bonds (Å)/angles (°)	0.007 / 1.132	0.0262 / 2.2276
Ramachandran plot, residues in:		
Most favored regions (%)	96.7	98.0
Additional allowed regions (%)	2.3	2.0
Generously allowed regions (%)	1.0	0
Disallowed regions (%)	0.0	0
PDB code	4LPI	5C6Y

[a] Numbers in parentheses represent values in the highest resolution shell (Å).

[b]  $R_{\text{sym}} = \sum |I_j - \langle I \rangle| / \sum I_j$ , where  $I_j$  is the observed integrated intensity,  $\langle I \rangle$  is the average integrated intensity obtained from multiple measurements, and the summation is over all observed reflections. [c]  $R_{\text{cryst}} = \sum ||F_{\text{obs}}| - |F_{\text{calc}}|| / \sum |F_{\text{obs}}|$ ,  $F_{\text{obs}}$  and  $F_{\text{calc}}$  are observed and calculated structure factor amplitudes, respectively.

[d]  $R_{\text{free}}$  calculated with randomly selected reflections (5%).